Peak-to-Average Power Ratio of OTFS modulation

G. D. Surabhi, Rose Mary Augustine, and Ananthanarayanan Chockalingam

***Abstract*—In this letter, we analyze the peak-to-average power ratio (PAPR) of orthogonal time frequency space modulation (OTFS) waveform. Towards this, we consider modulation symbols on an $N \times M$ delay-Doppler grid, where N and M are the number of Doppler and delay bins, respectively. We derive an upper bound on the PAPR of the OTFS signal and show that the maximum PAPR grows linearly with N (and not with M, the number of subcarriers, as observed in conventional multicarrier schemes such as OFDM). We analytically characterize the complementary cumulative distribution function (CCDF) of the PAPR of OTFS with rectangular pulse for large values of N. We present the simulated CCDF of the PAPR of OTFS for different pulse shapes and compare it with those of OFDM and generalized frequency division multiplexing (GFDM). It is shown that OTFS can have better PAPR compared to OFDM and GFDM.**

keywords: *OTFS modulation, delay-Doppler domain, peak-to-average power, OFDM, GFDM.*

I. Introduction

Orthogonal time frequency space (OTFS) modulation is a recently proposed two-dimensional (2-D) modulation technique which uses the delay-Doppler domain for multiplexing information symbols. OTFS uses pre- and post-processing operations on conventional multicarrier modulation schemes, resulting in improved bit error performance compared to conventional multicarrier techniques. Also, a rapidly time-varying multipath channel will exhibit slow variations in the delay-Doppler domain. That is, delay-Doppler representation of a multipath channel makes it time invariant for a longer duration compared to that in time-frequency representation. This can simplify the equalizer design and allow the channel to be estimated less frequently in OTFS, reducing the channel estimation overhead in a rapidly time-varying channel.

OTFS modulation was first introduced in [1], where it was shown to exhibit significantly superior error performances compared to OFDM systems for vehicle speeds as high as 500 km/h. Subsequently, several works on various aspects of OTFS modulation have emerged [2]-[8]. OTFS being a new modulation scheme, it is of interest to understand its PAPR characteristics. A formal PAPR characterization of OTFS has not been reported so far. In this letter, for the first time in the literature, we present an analysis of the PAPR performance of OTFS. An OTFS waveform in which MN information symbols are multiplexed across M delay bins and N Doppler bins is considered. For this waveform, we derive an analytical upper bound on the PAPR. This bound is found to increase linearly with the number of Doppler bins N and not with the number of delay bins M (or equivalently, the number of subcarriers in time-frequency domain). This is unlike in conventional multicarrier waveforms where the PAPR grows linearly with M. A consequence of this is that OTFS with $N < M$ (which typically is the case) can have a lower PAPR compared to a multicarrier system with M subcarriers. We also analytically characterize the complementary cumulative distribution function (CCDF) of the PAPR of OTFS for rectangular pulse shape. For other pulse shapes, simulation results of the CCDF are obtained. We compare the CCDF of the PAPR of OTFS with those of the OFDM and generalized frequency division multiplexing (GFDM) waveforms. Our results show that OTFS has better PAPR characteristics when $N < M$.

Manuscript received March 26, 2019; revised April 17, 2019; accepted April 20, 2019. The editor coordinating the review of this manuscript and approving it for publication was Dr. Mutlu Koca.

This work was supported in part by the J. C. Bose National Fellowship, Department of Science and Technology, Government of India, and by Tata Elxsi Limited, Bengaluru 560048, India.

The authors are with the Department of Electrical Communication Engineering, Indian Institute of Science, Bengaluru 560012, India (e-mail:surabhi@iisc.ac.in; rosemaryaugustine63@gmail.com; achockal@iisc.ac.in).

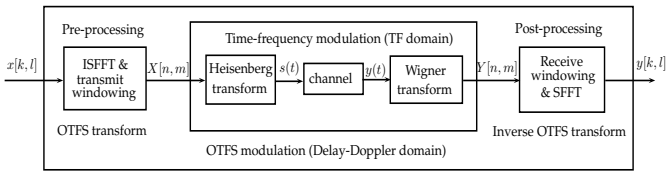

Fig. 1: OTFS modulation scheme.

II. System model

Figure 1 shows the block diagram of OTFS modulation architected over a general multicarrier modulation system. At the OTFS transmitter, the information symbols (e.g., QAM/PSK symbols) are treated as points in two dimensional delay-Doppler grid and are mapped to the time-frequency (TF) plane through the 2D inverse symplectic finite Fourier transform (ISFFT). The TF signal so obtained is then passed through a multicarrier modulation system. The TF signal is transformed to a time domain signal for transmission using Heisenberg transform. The output of the Heisenberg transform is transmitted over the linear time variant channel. At the receiver, the received time domain signal is transformed to TF domain using Wigner transform (inverse of Heisenberg transform) which are mapped back to delay-Doppler domain symbols using symplectic finite Fourier transform (SFFT).

At the transmitter, the time domain signal obtained as the output of Heisenberg transform has to be amplified before it is transmitted through the wireless channel. Hence, the PAPR of this time domain signal is of interest and has to be characterized. In the following subsection, we derive the expression for the discrete-time samples of the OTFS signal transmitted through the channel.

A. OTFS transmit signal

The transmitted signal in OTFS modulation in a given packet burst has a duration of NT and occupies a bandwidth $B = \frac{M}{T} = M\Delta f$. The information symbols denoted by $x[k,l]$, $k = 0, 1, \cdots, N-1$, $l = 0, 1, \cdots, M-1$ and $x[k,l] \in \mathbb{A}$, where $\mathbb{A}$ is the modulation alphabet (e.g., QAM/PSK), are

treated as points in the 2D delay-Doppler grid. The transmitter maps these symbols in the delay-Doppler domain to the time-frequency domain using the inverse symplectic finite Fourier transform (ISFFT), given by

$$X[n,m] = \sum_{k=0}^{N-1}\sum_{l=0}^{M-1} x[k,l]e^{-j2\pi(\frac{ml}{M}-\frac{nk}{N})}. \quad (1)$$

The time-frequency signal obtained as the output of ISFFT operation is then converted to time domain for transmission using the Heisenberg transform, given by

$$s(t) = \sum_{n=0}^{N-1}\sum_{m=0}^{M-1} X[n,m]g_{tx}(t-nT)e^{j2\pi m\Delta f(t-nT)}, \quad (2)$$

where $g_{tx}(t)$ is the transmit periodic prototype pulse shape of duration NT as in [8]. The discrete time representation of (2) can be obtained by sampling (2) with a sampling rate $F_s = \frac{1}{T_s} = B$ (Nyquist sampling), given by

$$s(uT_s) = \sum_{n=0}^{N-1}\sum_{m=0}^{M-1} X[n,m]g_{tx}(uT_s-nT)e^{j2\pi m\Delta f(uT_s-nT)}, \quad (3)$$

where $u = 0, 1, \cdots, MN-1$. We consider Nyquist sampling (oversampling ratio = 1) in the analysis. It is convenient to express the samples $s(u)$, $u = 0, 1, \cdots, MN-1$ as an $N \times M$ matrix with entries denoted by $s(q,r)$ such that $u = r + qM$, where $r = 0, 1, \cdots, M-1$ and $q = 0, 1, \cdots, N-1$. Substituting $u = r + qM$ and (1) in (3), we get

$$s(r+qM) = \sum_{n=0}^{N-1}\sum_{m=0}^{M-1}\sum_{k=0}^{N-1}\sum_{l=0}^{M-1} x[k,l]e^{-j2\pi(\frac{ml}{M}-\frac{nk}{N})} \cdot g_{tx}([r+qM-nM]_{MN})e^{j\frac{2\pi}{M}m(r+qM)}. \quad (4)$$

Here, mod-MN operation denoted by $[.]_{MN}$ confines the frame transmission within the duration NT [8]. Further, (4) can be simplified as

$$s(r+qM) = \sum_{k=0}^{N-1}\sum_{l=0}^{M-1} x[k,l]\sum_{m=0}^{M-1} e^{\frac{j2\pi m}{M}(-l+r)} \cdot \sum_{n=0}^{N-1} g_{tx}([r+qM-nM]_{MN})e^{\frac{j2\pi nk}{N}}. \quad (5)$$

Now, defining $\mathcal{F} \triangleq \sum_{m=0}^{M-1} e^{\frac{j2\pi m}{M}(-l+r)}$, we observe that

$$\mathcal{F} = \begin{cases} 0 & \text{if } r \neq l \\ M & \text{if } r = l. \end{cases} \quad (6)$$

Substituting (6) in (5), we get

$$s(r+qM) = M\sum_{n=0}^{N-1}\sum_{k=0}^{N-1} x[k,r]e^{\frac{j2\pi nk}{N}}g_{tx}([r+qM-nM]_{MN}). \quad (7)$$

Observe that $\sum_{k=0}^{N-1} x[k,r]e^{\frac{j2\pi nk}{N}}$ is the nth ($n = 0, 1, \cdots, N-1$) N-point IDFT of $x[k,r]$, $k = 0, 1, \cdots, N-1$, for a given r. Denoting $\tilde{x}_r[n] = \sum_{k=0}^{N-1} x[k,r]e^{\frac{j2\pi nk}{N}}$, (7) can be written as

$$s(r+qM) = M\sum_{n=0}^{N-1} \tilde{x}_r[n]g_{tx}([r+qM-nM]_{MN}). \quad (8)$$

III. PAPR in OTFS modulation

In this section, we derive an upper bound on the PAPR of OTFS transmit waveform and characterize the CCDF of the PAPR with rectangular pulse shape for large values of N.

A. Upper bound on PAPR

Consider the samples of transmitted OTFS signal in (8). The PAPR of the discrete-time samples of one frame of OTFS transmit signal is defined as

$$\text{PAPR} = \frac{\max_{r,q}\{|s(r+qM)|^2\}}{P_{\text{avg}}}, \quad (9)$$

where $P_{\text{avg}} = \frac{1}{MN}\sum_{r=0}^{M-1}\sum_{q=0}^{N-1} E\{|s(r+qM)|^2\}$. From (8), the numerator in (9) can be written as

$$\max_{r,q}|s(r+qM)|^2 = M^2\max_{r,q}\left|\sum_{n=0}^{N-1}\tilde{x}_r[n]g_{tx}([r+qM-nM]_{MN})\right|^2. \quad (10)$$

Using Cauchy-Schwarz inequality, (10) can be bounded as

$$\max_{r,q}|s(r+qM)|^2 \leq M^2\max_{r,q}\sum_{n=0}^{N-1}|\tilde{x}_r[n]|^2 \cdot \max_{r,q}\sum_{n=0}^{N-1}|g_{tx}([r+qM-nM]_{MN})|^2. \quad (11)$$

Recall that $\tilde{x}_r[n] = \sum_{k=0}^{N-1} x[k,r]e^{\frac{j2\pi nk}{N}}$, for a given r. Using Parseval's theorem, we can write

$$\max_{r}\sum_{n=0}^{N-1}|\tilde{x}_r[n]|^2 \leq N^2\max_{k,l}|x[k,l]|^2. \quad (12)$$

Therefore, substituting (12) in (11), we get

$$\max_{r,q}|s(r+qM)|^2 \leq M^2N^2\max_{k,l}|x[k,l]|^2 \cdot \max_{r,q}\sum_{n=0}^{N-1}|g_{tx}([r+qM-nM]_{MN})|^2. \quad (13)$$

Defining $B_1 \triangleq \max_{r,q}\sum_{n=0}^{N-1}|g_{tx}([r+qM-nM]_{MN})|^2$, (13) can be written as

$$\max_{r,q}|s(r+qM)|^2 \leq M^2N^2\max_{k,l}|x[k,l]|^2B_1. \quad (14)$$

Now, the denominator in (9) can be written as

$$P_{\text{avg}} = \frac{M^2}{MN}\sum_{r=0}^{M-1}\sum_{q=0}^{N-1} E\Big\{|\sum_{n=0}^{N-1}\tilde{x}_r[n]g_{tx}([r+qM-nM]_{MN})|^2\Big\}. \quad (15)$$

Note that for a given value of r, $\tilde{x}_r[n]$s are IDFT values of $x[k,r]$, $k = 0, 1, \cdots, N-1$. Since $x[k,l]$s are information symbols from a modulation alphabet $\mathbb{A}$, they can be treated i.i.d. with zero mean and variance $\sigma_a^2 = E\{|x[k,l]|^2\}$. Also, due to the Nyquist sampling of the transmit signal, the samples $\tilde{x}_r[n]$s are mutually uncorrelated and hence (15) can be simplified as

$$P_{\text{avg}} = \frac{M^2}{MN}\sum_{r=0}^{M-1}\sum_{q=0}^{N-1}\sum_{n=0}^{N-1}E\{|\tilde{x}_r[n]|^2\}|g_{tx}([r+qM-nM]_{MN})|^2. \quad (16)$$

Observe that $E\{|\tilde{x}_r[n]|^2\} = N\sigma_a^2, \ \forall\ r, n$. With this, (16) can be further simplified as

$$P_{\text{avg}} = \frac{M^2N\sigma_a^2}{MN}\sum_{n=0}^{N-1}\sum_{r=0}^{M-1}\sum_{q=0}^{N-1}|g_{tx}([r+qM-nM]_{MN})|^2. \quad (17)$$

Defining $B_2 \triangleq \frac{1}{MN}\sum_{n=0}^{N-1}\sum_{r=0}^{M-1}\sum_{q=0}^{N-1}|g_{tx}([r+qM-nM]_{MN})|^2$, the PAPR of OTFS transmit signal can be upper bounded as

$$\text{PAPR} \leq \frac{M^2N^2 \max_{k,l}|x[k,l]|^2 B_1}{M^2N\sigma_a^2 B_2} = \frac{N \max_{k,l}|x[k,l]|^2 B_1}{\sigma_a^2 B_2}. \tag{18}$$

Note that (18) is a bound on the PAPR of transmit signal in OTFS with any pulse shape $g_{tx}(t)$. Now, consider OTFS with rectangular pulse shape. In this case $B_1/B_2 = 1$, and hence the maximum PAPR will meet the bound in (18), i.e.,

$$\text{PAPR}_{\text{max}} = \frac{N \max_{c\in\mathbb{A}}|c|^2}{\sigma_a^2}. \tag{19}$$

Note that the upper bound on the PAPR of OTFS transmit signal grows linearly with N and not with M. This is an interesting feature of OTFS modulation compared to other multicarrier modulations where the PAPR depends on the number of subcarriers (M) and grows linearly with the number of subcarriers used. In practice, the number of delay bins/subcarriers (M) is chosen such that $\Delta f = B/M$ satisfies $\nu_{\text{max}} < \Delta f < 1/\tau_{\text{max}}$, where τ_{max} and ν_{max} denote the maximum delay and Doppler spread of the channel, respectively. The value of N decides the Doppler resolution and it is generally chosen such that the maximum latency constraint of the application is satisfied (larger N results in larger decoding delay). Hence, in practice N is less than M.

B. CCDF of PAPR

While the maximum PAPR analysis presented above is of interest, it is also important to characterize the CCDF of PAPR. For the ease of analysis, we consider OTFS modulation with rectangular pulse. From (8), it can be seen that the time domain samples of the OTFS transmit signal with rectangular pulse are nothing but the N-point IDFT values of the symbols in the delay-Doppler domain. Hence, if N is large, then by central limit theorem, the transmitted samples can be approximated to have complex Gaussian distribution with zero mean [9]. Therefore, the instantaneous envelope $|s[u]|$ is Rayleigh distributed and hence the instantaneous-to-average power ratio (IAPR = $|s[u]|^2/E\{|s|^2\}$) of each time domain sample follows exponential distribution. Therefore, the probability that the IAPR does not exceed a threshold γ_0 is given by

$$P(\text{IAPR} \leq \gamma_0) \approx (1 - e^{-\gamma_0}). \tag{20}$$

Assuming the transmitted samples to be mutually uncorrelated, which is true for Nyquist sampling (oversampling ratio=1), the probability that the PAPR of the transmit OTFS signal in a frame does not exceed γ_0 is given by

$$P\left(\text{PAPR} \leq \gamma_0\right) \approx \prod_{i=0}^{NM-1}\left(1 - e^{-\gamma_0}\right) = \left(1 - e^{-\gamma_0}\right)^{MN}. \tag{21}$$

Note that the assumption that the transmitted samples are uncorrelated does not hold when the transmit signal is oversampled [10]. Now, the CCDF of PAPR is given by

$$P\left(\text{PAPR} > \gamma_0\right) \approx 1 - \left(1 - e^{-\gamma_0}\right)^{MN}. \tag{22}$$

Note that the PAPR in OTFS is bounded by PAPR_{max} derived in Sec. III-A, i.e., $P(\text{PAPR} > \gamma_0) = 0$ for $\gamma_0 > \text{PAPR}_{\text{max}}$. However, the CCDF in (22) does not capture this. Hence, (22) is an approximation to the actual CCDF. The actual CCDF of PAPR converges to the CCDF in (22) as $N \to \infty$.

IV. Results and discussions

Figure 2a shows the simulated CCDF of IAPR of the transmitted OTFS signal with rectangular pulse and Nyquist sampling (oversampling ratio=1) using 4-QAM for $M = 32, 256$ and $N = 32, 128$. We also plot the analytical CCDF of IAPR using (20). From Fig. 2a, we observe that the simulated CCDF gets closer to the analytical CCDF for higher values of N, indicating that the transmitted samples attain Gaussian distribution as N grows. Note that the CCDF of IAPR does not depend on M. Next, Fig. 2b shows the CCDF of PAPR for OTFS modulation with rectangular pulse for systems with $M = 256$ and $N = 4, 8, 32, 128$, and 256. All the systems use 4-QAM modulation and Nyquist sampling. The simulated CCDF of PAPR along with the analytical CCDF in (22) for all the systems are plotted. We see that the simulated CCDF matches very closely with the analytical CCDF in (22) for higher values of N, indicating that the analytical CCDF is more accurate in the large N regime. We also observe that the systems with smaller value of N have lower PAPR and the PAPR increases with increase in the value of N. Hence, it is evident that the maximum PAPR in OTFS modulation grows with N, as inferred from the upper bound in Sec. III-A.

Effect of increasing M and N on CCDF of PAPR: Figure 3 shows the CCDF of PAPR of OTFS with $M = 32, 64$, and 128 for $N = 4$ and $N = 8$. All the systems use 4-QAM and Nyquist sampling. From Sec. III-A, PAPR_{max} depends only on N and grows linearly with N. The maximum PAPR with $N = 4$ and 8 is $10\log 4 = 6.02$ dB and $10\log 8 = 9.03$ dB, respectively. From Fig. 3, we observe that the CCDF is zero for $\gamma_0 > 6.02$ dB for $N = 4$ and $\gamma_0 > 9.03$ dB for $N = 8$. Also, with increase in the value of M, the probability to have large peaks increases, and hence the CCDF of PAPR increases, as indicated by (22). Therefore, although increasing M increases the CCDF, the maximum PAPR depends only on N and $P(\text{PAPR} > \gamma_0) = 0$ for $\gamma_0 > \text{PAPR}_{\text{max}}$.

Effect of pulse shaping on PAPR: OTFS uses bi-orthogonal pulses which are well localized in time and frequency at the transmitter and the receiver to suppress ISI and ICI in the time-frequency plane. Hence it is important to study the PAPR of OTFS with different pulse shapes. Figure 4 shows the comparison of the CCDF of PAPR with $M = 256$, $N = 8$ with $i)$ rectangular pulse defined as $\text{rect}(t/T)$, $ii)$ raised cosine (RC) pulse defined as $\frac{\text{sinc}(t/T)\cos(\pi a t/T)}{(1-4a^2(t/T)^2)}$ with $a = 0.5$, and $iii)$ Gaussian pulse defined as $e^{-a\pi(t/T)^2}$ with $a = 1$, for $-NT/2 \leq t < NT/2$. All the pulses are sampled at a rate $1/T_s$ to obtain MN discrete time samples which are normalized to have unit energy. All the systems use 16-QAM and are four times oversampled using an RC filter of length $6T$ with a roll-off factor of 0.5. From Fig. 4, we observe that the PAPR of OTFS with pulse shaping can increase as indicated by the upper bound in (18). We see that OTFS with rectangular pulse has a better PAPR compared to that of RC pulse which in turn has a better PAPR compared to Gaussian pulse.

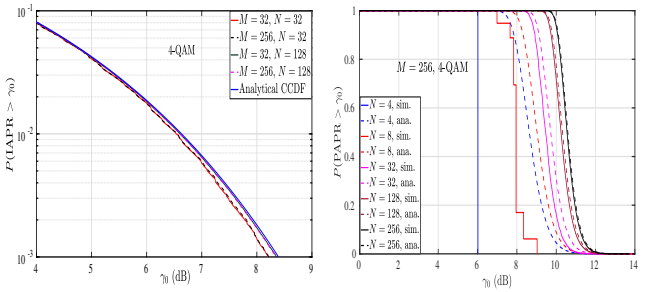

(a) CCDF of IAPR in OTFS. (b) CCDF of PAPR in OTFS.

Fig. 2: Analytical and simulated CCDF of IAPR and PAPR.

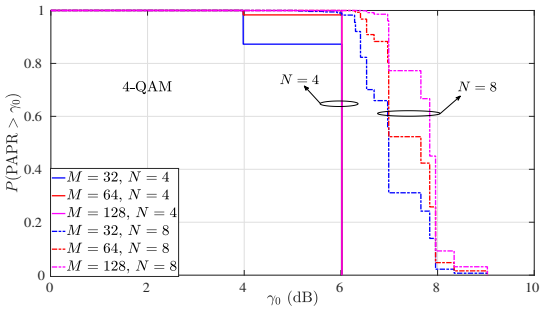

Fig. 3: Effect of M and N on the CCDF of PAPR in OTFS.

Comparison with GFDM and OFDM: GFDM is a block based time-frequency multicarrier transmission scheme that offers flexible pulse shaping of individual subcarriers [11]. The transmit waveform of GFDM follows (3) in which $X[n,m]$s are the information symbols from the modulation alphabet $\mathbb{A}$. OFDM can be viewed as a special case of GFDM where the pulse shape is rectangular and $N = 1$. In Fig. 5, we compare the CCDF of the PAPR of OTFS with those of GFDM and OFDM systems with $M = 256, N = 4$ and $M = 256, N = 32$. All the systems use 16-QAM and an oversampling ratio of four is used. For all the considered systems, oversampling is done using an RC filter of length $6T$ and roll-off factor 0.5. Note that, for comparison of M-subcarrier OFDM with OTFS and GFDM, which have MN symbols in a frame, we consider the CCDF of concatenation of N OFDM symbols. From Fig. 5, we observe that, for the same number of subcarriers, OFDM has a slightly better PAPR compared to GFDM, as was also shown in [12],[13]. We also observe that OTFS with rectangular pulse can have better PAPR compared to OFDM and GFDM (using RC pulse shaping with roll-off factor 0.5) systems. For example, OTFS with $N = 4$ has a PAPR which is approximately 2.2 dB lower than that of OFDM and approximately 2.4 dB lower than that of GFDM at a probability of 10^{-3}. However, increasing N to 32 shifts the CCDF of OTFS closer to that of GFDM and OFDM and the gain in PAPR compared to that of OFDM reduces to 0.3 dB at a probability of 10^{-3}. Therefore, as seen in Sec. III-A, the maximum PAPR in OTFS increases with N, and hence OTFS can have better PAPR compared to OFDM and GFDM when $N < M$. This demonstrates the good PAPR characteristics of the OTFS waveform.

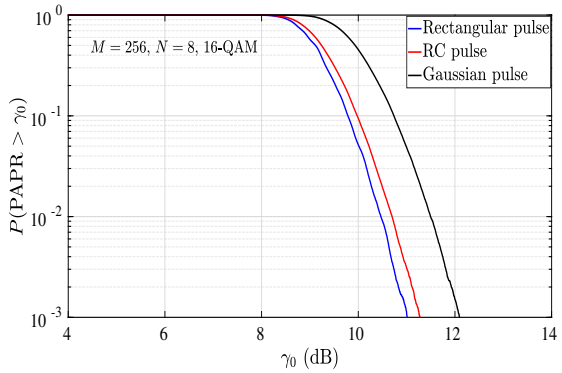

Fig. 4: CCDF of the PAPR of OTFS for different pulse shapes.

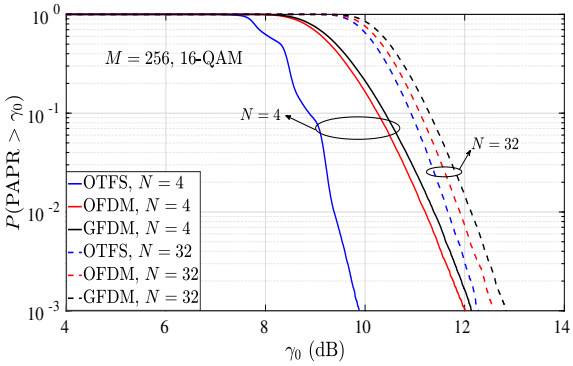

Fig. 5: Comparison of CCDF of the PAPR of OTFS with those of OFDM and GFDM with 16-QAM.

REFERENCES

[1] R. Hadani, S. Rakib, M. Tsatsanis, A. Monk, A. J. Goldsmith, A. F. Molisch, and R. Calderbank, "Orthogonal time frequency space modulation," in *Proc. IEEE WCNC'2017*, Mar. 2017, pp. 1-7.

[2] A. Monk, R. Hadani, M. Tsatsanis, and S. Rakib, "OTFS - orthogonal time frequency space: a novel modulation technique meeting 5G high mobility and massive MIMO challenges," online: arXiv:1608.02993 [cs.IT] 9 Aug 2016.

[3] R. Hadani, S. Rakib, S. Kons, M. Tsatsanis, A. Monk, C. Ibars, J. Delfeld, Y. Hebron, A. J. Goldsmith, A. F. Molisch, and R. Calderbank, "Orthogonal time frequency space modulation," online: arXiv:1808.00519v1 [cs.IT] 1 Aug 2018.

[4] R. Hadani, S. Rakib, A. F. Molisch, C. Ibars, A. Monk, M. Tsatsanis, J. Delfeld, A. Goldsmith, and R. Calderbank, "Orthogonal time frequency space (OTFS) modulation for millimeter-wave communications systems," in *Proc. IEEE MTT-S Intl. Microwave Symp.*, pp. 681-683, Jun. 2017, pp. 681-683.

[5] K. R. Murali and A. Chockalingam, "On OTFS modulation for high-Doppler fading channels," in *Proc. ITA'2018*, San Diego, Feb. 2018.

[6] A. Farhang, A. R. Reyhani, L. E. Doyle, and B. Farhang-Boroujeny, "Low complexity modem structure for OFDM-based orthogonal time frequency space modulation," *IEEE Wireless Commun. Lett.*, vol. 7, no. 3, pp. 344-347, Jun. 2018.

[7] P. Raviteja, Y. Hong, E. Viterbo, and E. Biglieri, "Practical pulse shaping waveforms for reduced-cyclic-prefix OTFS," *IEEE Trans. Veh. Tech.*, vol. 68, no. 1, pp. 957-961, Jan. 2019.

[8] A. Nimr, M. Chafii, M. Matthe, and G. Fettweis, "Extended GFDM framework: OTFS and GFDM comparison," online: arXiv:1808.01161v1 [eess.SP] 3 Aug 2018.

[9] A. Goldsmith, *Wireless Communications*, Cambridge Univ. press, 2005.

[10] R. V. Nee and R. Prasad, *OFDM for Wireless Multimedia Communications*, Artech House, 2000.

[11] N. Michailow, M. Matthe, I. S. Gaspar, A. N. Caldevilla, L. L. Mendes, A. Festag, and G. Fettweis, "Generalized frequency division multiplexing for 5th generation cellular networks," *IEEE Trans. Commun.*, vol. 62, no. 9, pp. 3045-3061, Sep. 2014.

[12] S. S. Das and S. Tiwari, "Discrete Fourier transform spreading-based generalised frequency division multiplexing," *Electron. Lett.*, vol. 51, no. 10, pp. 789-791, May 2015.

[13] S. B. Slimane, "Peak-to-average power ratio reduction of OFDM signals using pulse shaping," in *Proc. IEEE GLOBECOM'2000*, Dec. 2000, pp. 1412-1416.